Cumulative and Transient Surface Deformation Signals in the Permian Basin

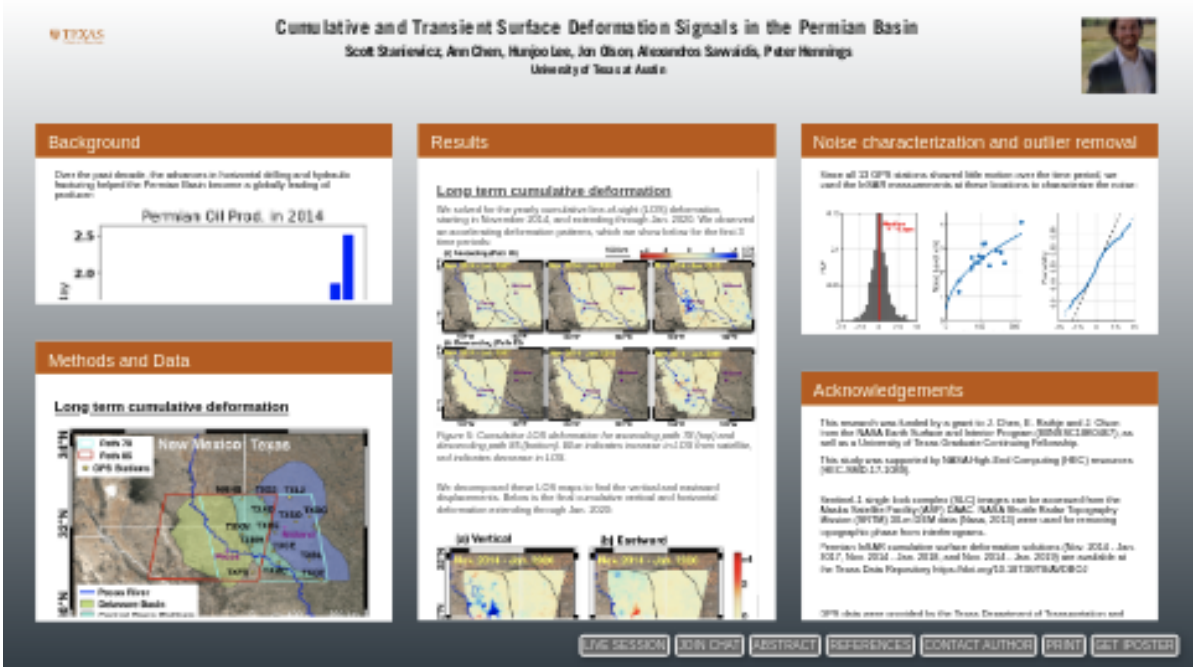

Scott Staniewicz, Ann Chen, Hunjoo Lee, Jon Olson, Alexandros Savvaidis, Peter Hennings

University of Texas at Austin

PRESENTED AT:

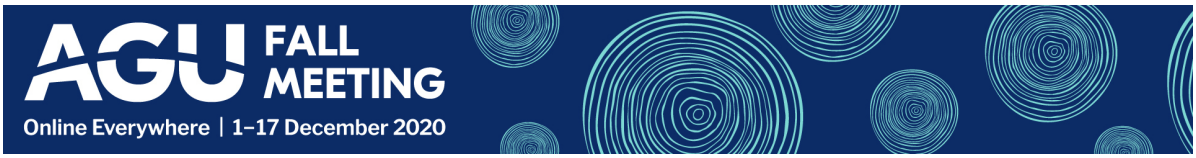

BACKGROUND

Over the past decade, the advances in horizontal drilling and hydraulic fracturing helped the Permian Basin become a globally leading oil producer:

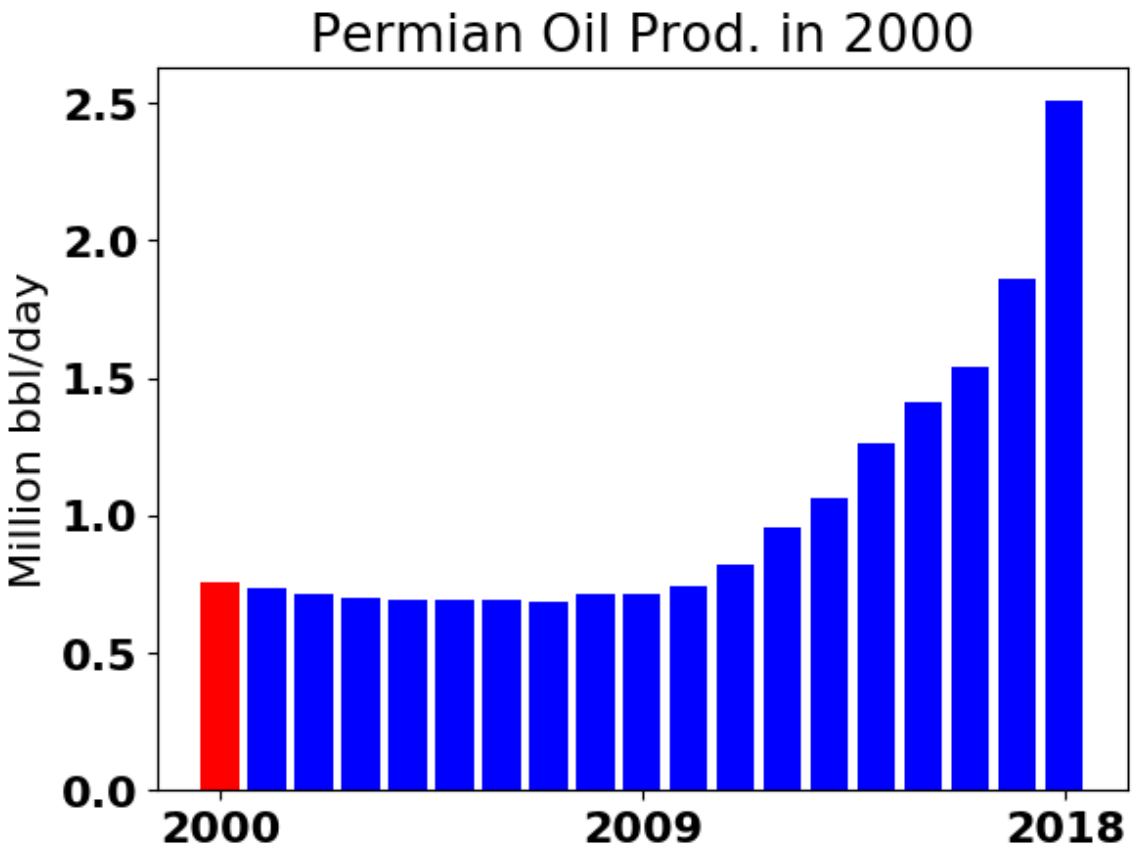

Figure 1: Yearly oil production rate in the Permian Basin (in millions of barrels per day), as reported by the Texas Railroad Commision.

During the same time period, West Texas has seen a large rise in the number of low magnitude earthquakes. Here we see the number of earthquakes per year as detected by the TXAR seismic array:

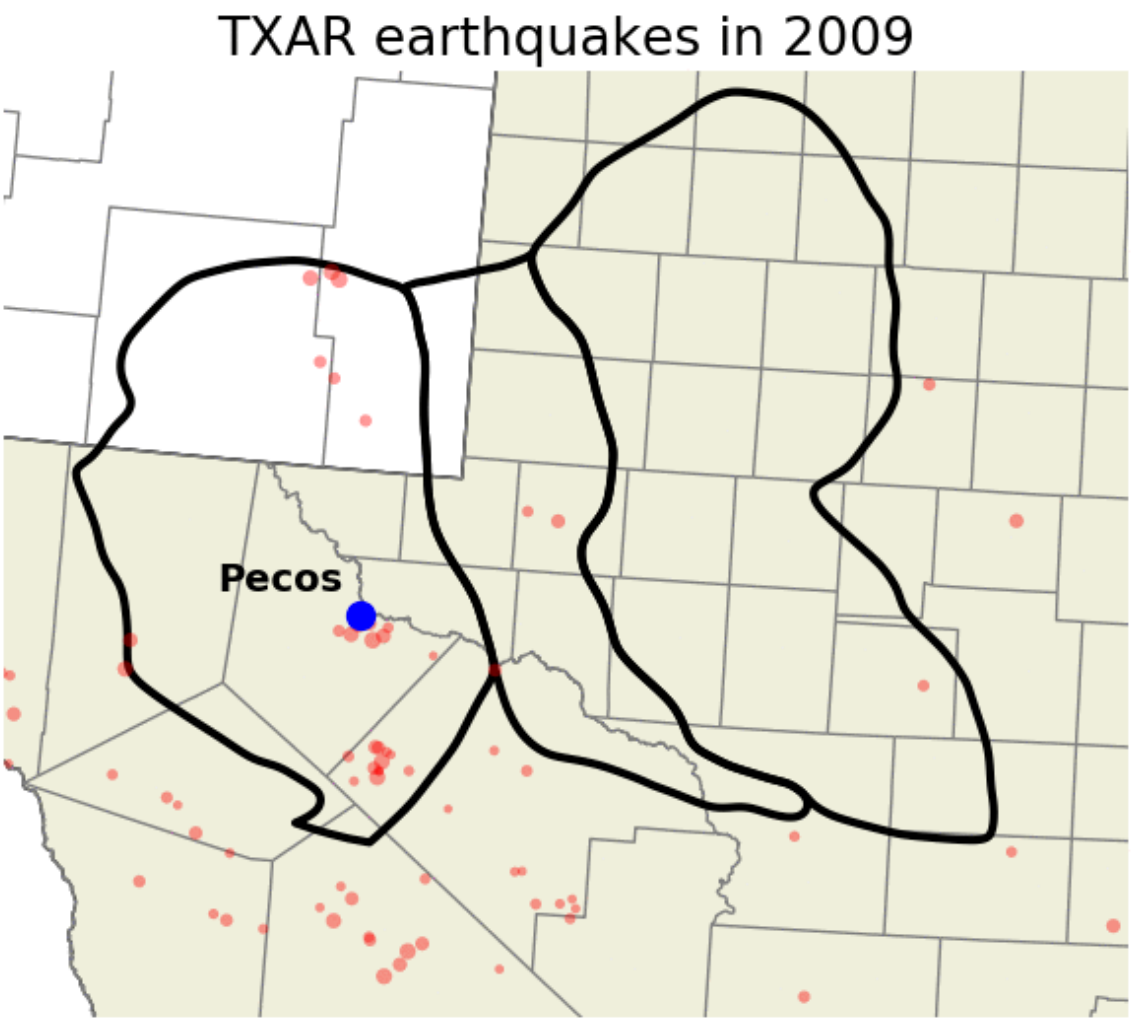

Figure 2: Yearly TXAR-detected earthquake hypocenters, as reported in [1].

Below we see the spatial extent of the oil production (b) and wastewater injection (e). Despite the widespread activities, the earthquakes are clustered spatially (d).

A detailed knowledge of changes to the subsurface can aid in understanding the causes of seismicity, and these changes can be inferred from InSAR surface deformation measurements

METHODS AND DATA

Long term cumulative deformation

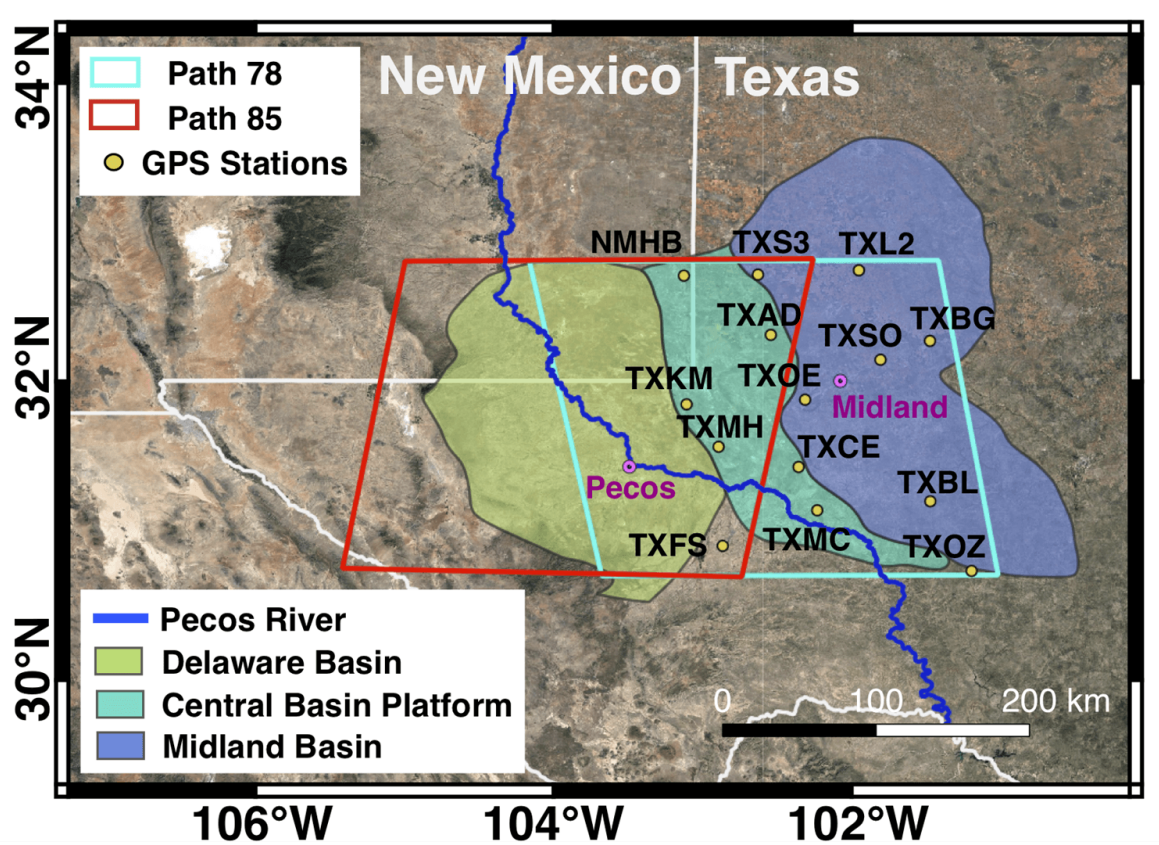

Figure 3: Study area for the cumulative long term deforamtion study in [2], showing ascending and descending Sentinel-1 data footprint and available GPS permanent stations.

Using a Sentinel-1 geocoded SLC processor [2] we processed >100 scenes from ascending (path 78, frames 94-104) and descending path 85 (frames 483- 493) acquired between Nov. 2014 and Jan. 2020.

We generated more than 10,000 interferograms at 120 meter pixel spacing and a maximum temporal baseline of 800 days. We were able to unwrap all interferograms without additional spatial filtering using the Statistical-cost, Network-flow Algorithm for Phase Unwrapping (SNAPHU). We removed long-wavelength phase ramps using a planar phase model.

We processed 14 permanent GPS stations (Figure 1) that recorded daily east, north, and up (ENU) surface deformation measurements. We used the area near TXKM as our InSAR reference point and, the remaining 13 stations served as validation points.

To solve for cumulative deformation, we compared InSAR LOS deformation solutions as derived from (1) the stacking method, (2) a SBAS linear deformation model with L1 and L2-norm penalty functions, and (3) unregularized and regularized SBAS deformation time series (Staniewicz et. al, 2020; Supporting Information S5).

Mentone coseismic deformation

We also processed 20 scenes of data from ascending path 151 near the M4.9 Mentone earthquake (in red):

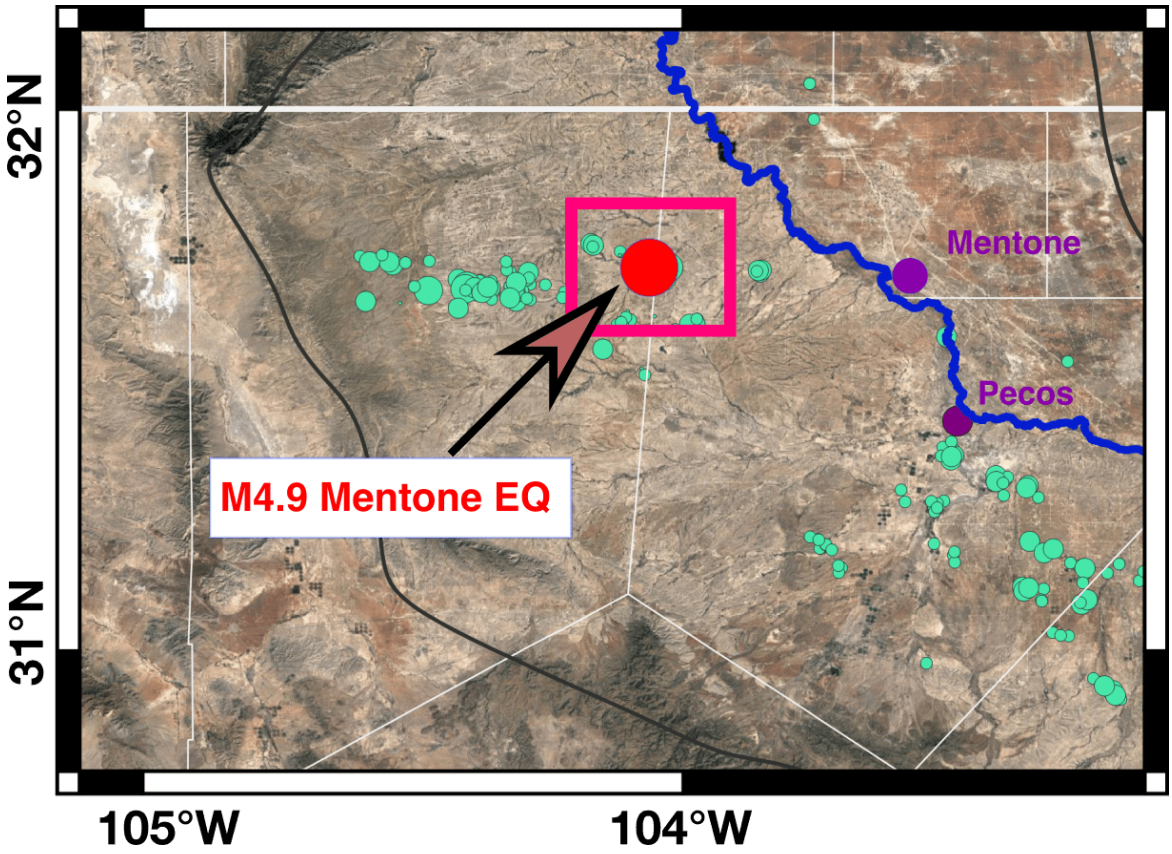

Figure 4: Study area for coseismic InSAR analysis of the 2020-03-26 M4.9 Mentone earthquake. Red box indicates InSAR study area, green dots indicate early 2020 TexNet-detected earthquakes.

To detect coseismic deformation from this event, we used a different processing strategy from the cumulative results. We averaged a stack of 10 independent interferograms formed from the 20 SAR images, where each independent interferogram spaned the event. Assuming the signal is a transient, step-like offset, each interferogram should contain the same earthquake signal, and the independent stacking would average out tropospheric noise.

RESULTS

Long term cumulative deformation

We solved for the yearly cumulative line-of-sight (LOS) deformation, starting in November 2014, and extending through Jan. 2020. We observed an accelerating deformation patterns, which we show below for the first 3 time periods:

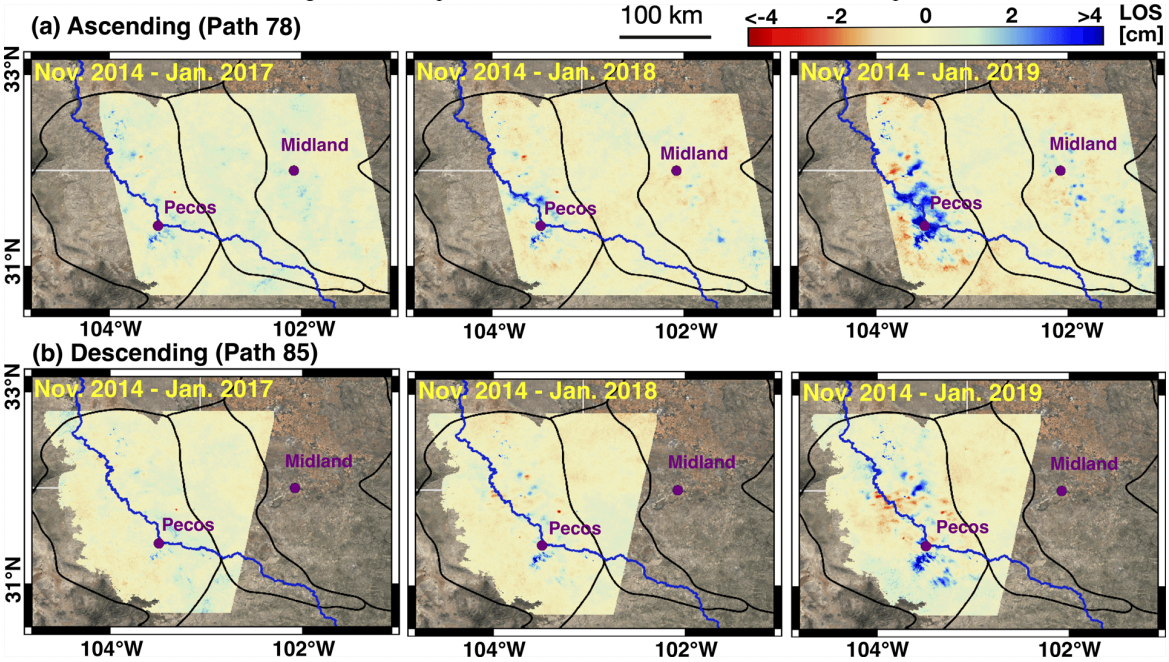

Figure 5: Cumulative LOS deformation for ascending path 78 (top) and descending path 85 (bottom). Blue indicates increase in LOS from satellite, red indicates decrease in LOS.

We decomposed these LOS maps to find the vertical and eastward displacements. Below is the final cumulative vertical and horizontal deformation extending through Jan. 2020:

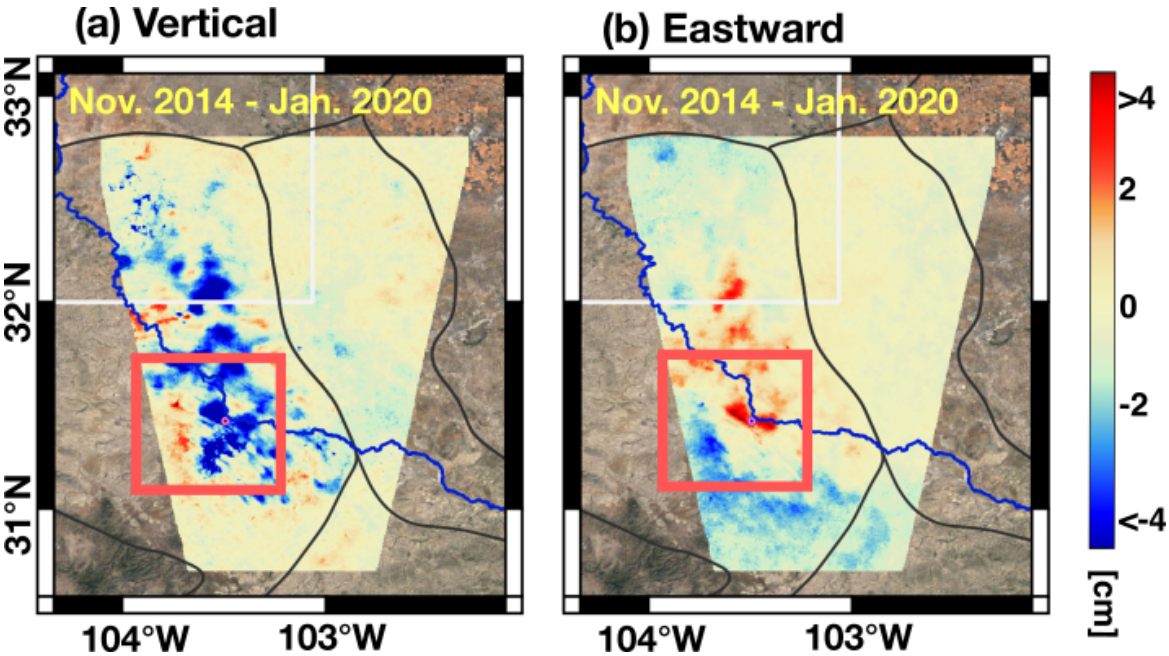

Figure 6: Cumulative vertical (left) and horizontal (right) deformation between Nov. 2014 and Jan. 2020.

We found that the linear features in the southern Delaware Basin aligned with the Texnet detected earthquake hypocenters:

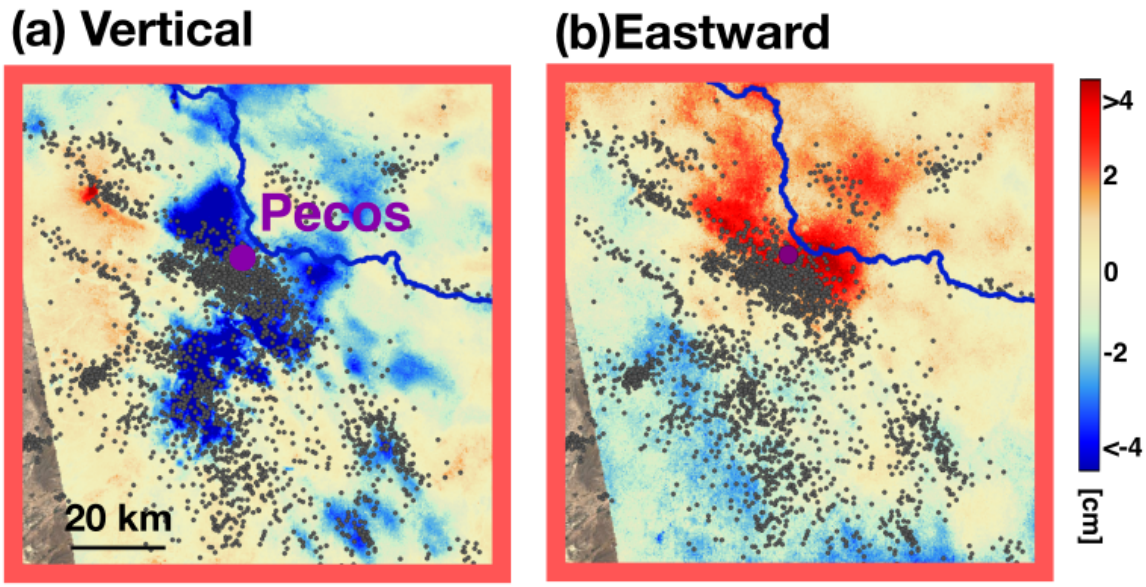

Figure 7: Pecos area cumulative vertical deformation with 2018 TexNet detected earthquakes.

Mentone coseismic deformation

Using the independent stacking approach, we found a ~7mm signal near with the M4.9 Mentone earthquake hypocenter. The red dot indicates the M4.9 earthquake hypocenter, green dots indicate other nearby Texnet-detected earthquakes from early 2020:

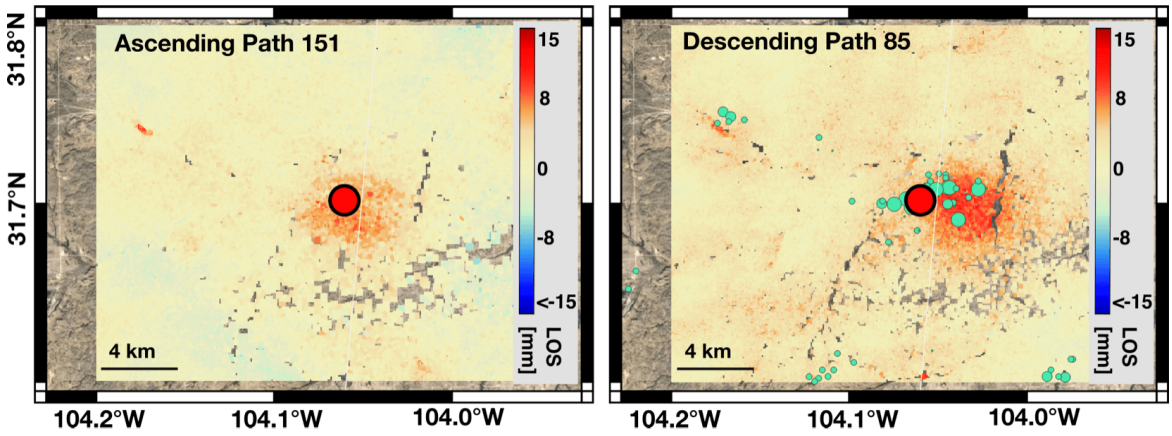

Figure 8: Ascending (left) and descending (right) detected LOS coseismic deformations from the 2020-03-26 M4.9 earthquake (red dot).

NOISE CHARACTERIZATION AND OUTLIER REMOVAL

Since all 13 GPS stations showed little motion over the time period, we used the InSAR measurements at these locations to characterize the noise:

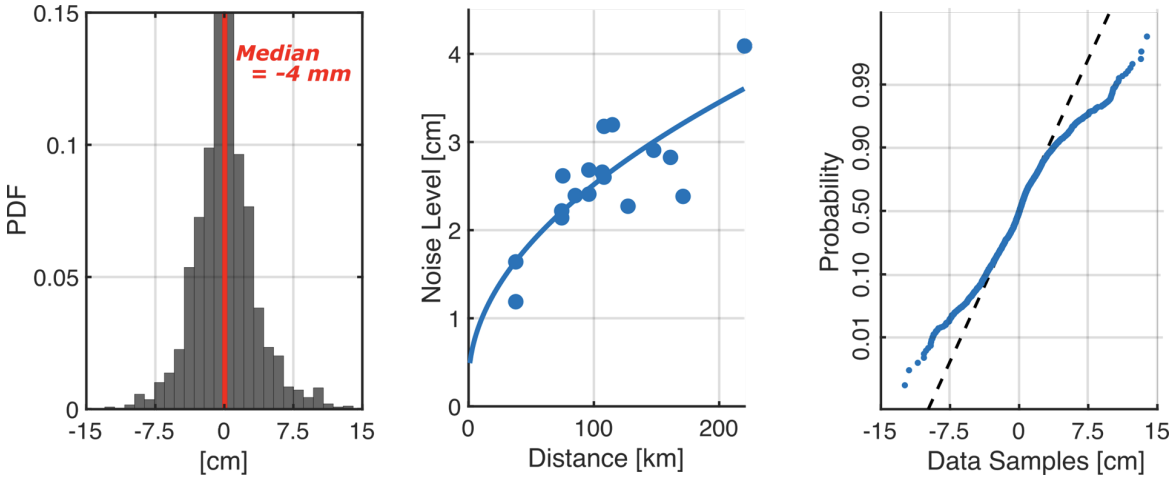

Figure 9: Noise characterization based on InSAR measurements at GPS control points showing spread of noise (left), growth with distance (middle), and heavy tails of distribution (right).

At the example station TXMC (left) we see a histogram of noise InSAR values. The noise is centered around 0 with a standard deviation of 3.2 cm. The middle panel shows that the noise grows with the square root of distance to the reference station.

The right plot is a probability plot (Filliben, 1975), which compares the observed noise distribution to a normal distribution. The deviation from the straight line shows that the tails of the observed data are significantly non-Gaussian, with a higher kurtosis.

We performed a pixel-wise outlier removal to mitigate the SAR dates with the most severe tropospheric noise. We measured a 2x reduction in uncertainty, as compared with 13 GPS validation points, down to 1-3mm/year across the Permian Basin:

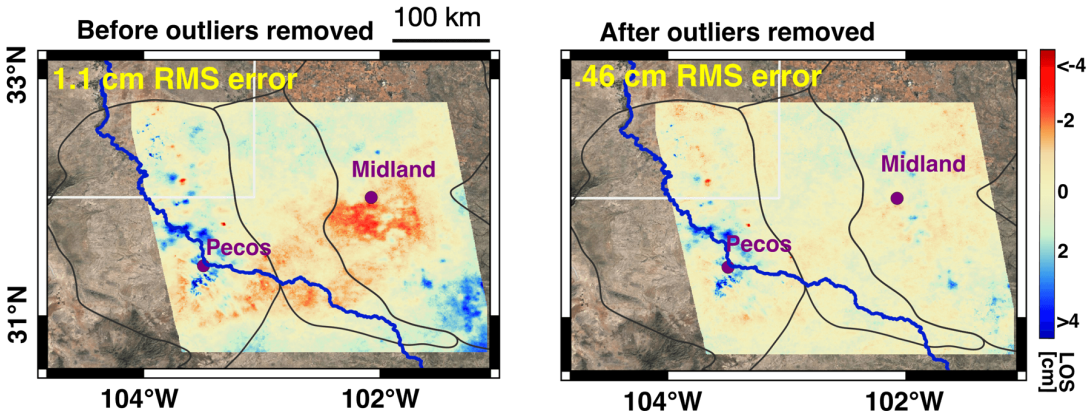

Figure 10: Visual and quantitative comparison of tropospheric artifacts before (left) and after (right) performing pixelwise outlier removal.

Additionally, all time series methods we compared showed an improvement after including our outlier removal:

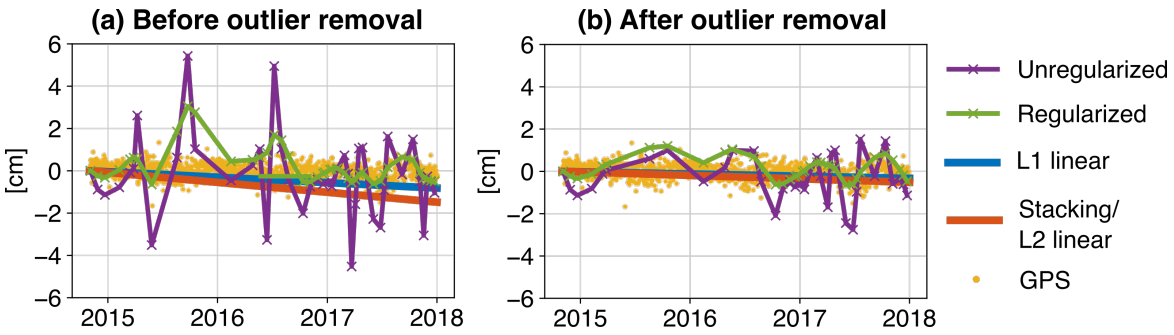

Figure 11: Comparison of timeseries methods before (left) and after (right) performing pixelwise the outlier removal at GPS station TXSO.

For our coseismic stacking results, we used similar ideas to detect large tropospheric noise, but calculated the test statistics on the entire image patches (~15 x 15 km) instead of on individual pixels.

Below we illustrate our method for detecting bad dates.

Given the 20 SAR dates around the Mentone earthquake, we formed all possible interferograms from SAR images. We then form the "average interferogram" for each SAR date:

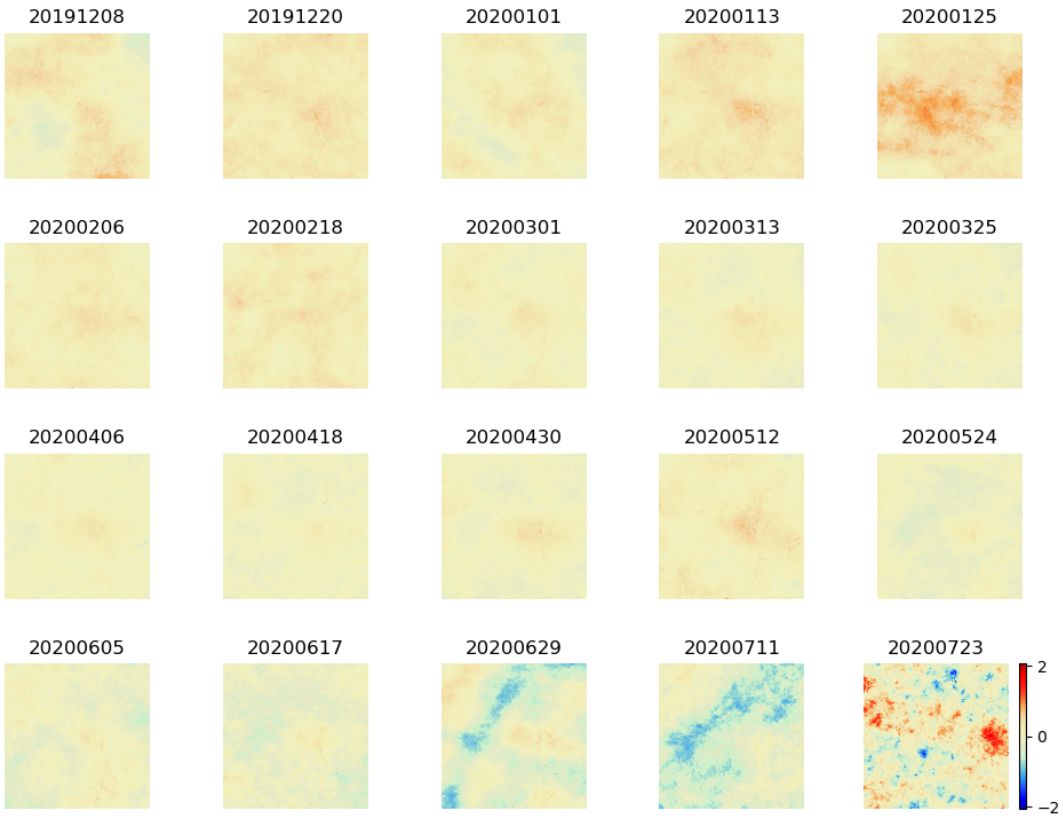

Figure 12: Plots of "average interferograms" for 20 SAR images around the 2020-03-26 event date. Image region is outlined in

second part of "Methods and Data" overview.

Since atmospheric noise is different on each date and is present in all interferograms containing that date, the average images here are a good indication of the tropospheric noise.

Some dates are visually contain much more tropospheric noise. Since the patch is small (~15 km x 15 km), we can take the variance over each image. This yields a timeseries with an obvious outlier, where the final date has variance of 0.24 compared to the median variance of ~0.02.

We compared the result of stacking the indepdent interferograms spanning the earthquake including (before) and excluding (after) the final noisy SAR date:

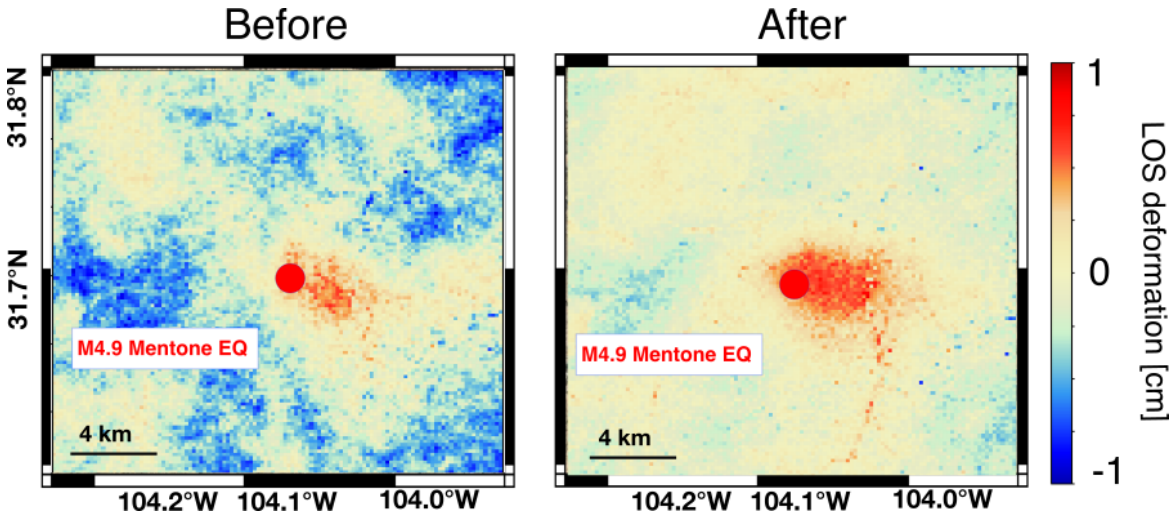

Figure 13: Coseismic stack results before (left) and after (right) detecting and removing outlier tropospheric noise dates from the average SAR interferograms.

ACKNOWLEDGEMENTS

This research was funded by a grant to J. Chen, E. Rathje and J. Olson from the NASA Earth Surface and Interior Program (80NSSC18K0467), as well as a University of Texas Graduate Continuing Fellowship.

This study was supported by NASA High-End Computing (HEC) resources (HEC-SMD-17-1089).

Sentinel-1 single look complex (SLC) images can be accessed from the Alaska Satellite Facility (ASF) DAAC. NASA Shuttle Radar Topography Mission (SRTM) 30-m DEM data (Nasa, 2013) were used for removing topographic phase from interferograms.

Permian InSAR cumulative surface deformation solutions (Nov. 2014 - Jan. 2017, Nov. 2014 - Jan. 2018, and Nov. 2014 - Jan. 2019) are available at the Texas Data Repository https://doi.org/10.18738/T8/AVDBOJ

GPS data were provided by the Texas Department of Transportation and processed by the Nevada Geodetic Laboratory (http://geodesy.unr.edu/) (Blewitt et al., 2018).

The TexNet earthquake catalog is available at http://www.beg.utexas.edu/texnet/catalog

Mapping figures were created using the QGIS software (Team et al., 2020).

ABSTRACT

The Permian Basin has become the United States' largest producer of oil over the past decade. Along with the rise in production, there has been an increase in the rate of low magnitude earthquakes, some of which have been associated with hydrocarbon extraction and wastewater injection. A detailed knowledge of changes to the subsurface can aid in understanding the causes of seismicity, and these changes can be inferred from InSAR surface deformation measurements.

In this study, we show that both cm-level cumulative deformation, as well as mm-level coseismic deformation signals, are detectable in West Texas. In a region west of Mentone, TX, we reconstructed the subtle coseismic deformation signal on the order of ~5 mm associated with the recent M4.9 earthquake. Over ~100,000 km^2 of the Permian Basin, we created annual cumulative LOS deformation maps, decomposing into vertical and eastward components where overlapping data are available. These maps contain numerous subsidence and uplift features near active production and disposal wells. The most important deformation signatures are linear streaks that extend tens of kilometers near Pecos, TX, where a cluster of increased seismic events was cataloged by TexNet. As validated by independent GPS data, our InSAR processing strategy achieved millimeter-level accuracy.

A careful treatment of the InSAR tropospheric noise, which can be as large as 15 cm in West Texas, is required to detect surface deformation signals with such low signal-to-noise ratio. We developed an outlier removal technique based on robust statistics to detect the presence of strong, non-Gaussian noise. We compared the surface deformation solutions of multiple InSAR time series methods, and all of them produced more accurate and consistent deformation trends after removing outlier InSAR measurements. We are exploring a Bayesian generalization of SBAS velocity estimation by including probabilistic data rejection to determine which pixels should be excluded from the model fitting. This technique provides a full posterior distribution of the model parameters along with the best-fit surface velocity.

REFERENCES

[1] Frohlich, C., Hayward, C., Rosenblit, J., Aiken, C., Hennings, P., Savvaidis, A., . . . DeShon, H. R. (2019). Onset and cause of increased seismic activity near pecos, west texas, usa from observations at the lajitas txar seismic array. Jour- nal of Geophysical Research: Solid Earth.

[2] Staniewicz, S., Chen, J., Lee, H., Olson, J., Savvaidis, A., Reedy, R., et al. (2020). InSAR reveals complex surface deformation patterns over an 80,000 km2 oil-producing region in the Permian Basin. Geophysical Research Letters, 47, e2020GL090151. https://doi-org.ezproxy.lib.utexas.edu/10.1029/2020GL090151

[3] Zheng, Y., & Zebker, H. A. (2017). Phase correction of single-look complex radar images for user-friendly efficient interferogram formation. IEEE Journal of Selected Topics in Applied Earth Observations and Remote Sensing, 10(6), 2694–2701.

[4] Staniewicz, Scott; Jingyi Chen, 2020, "InSAR Surface Deformation Data over Permian Basin from Staniewicz et al. (2020), Geophysical Research Letters", https://doi.org/10.18738/T8/AVDBOJ, Texas Data Repository Dataverse, V6